Quantification of defect size in shearing direction by shearography and wavelet transform

Fabrice Michel[a,b], Vincent Moreau[a], Vanessa Rosso[b], Serge Habraken[b] and Bernard Tilkens[a]

[a] DEIOS s.a, Liege Science Park - Spatiopôle, rue des chasseurs ardennais, 4 (WSL), 4031 Angleur, Belgium;

[b] HOLOLAB, Department of Physics, Bat. B5a, Université de Liège, 4000 Liège, Belgium

ABSTRACT

Shearography is a recognized interferometric technique in non-destructive testing to detect defects. Defects are detectable in wrapped phase maps because they are characterized in their neighborhood by singular fringes. They are detectable in unwrapped phase maps, because they induce unexpected phase values. By analyzing the length of unexpected phase values area in shearing direction, and by taking into consideration shearing amount, defect size can be locally estimated. To examine this length, we propose to locally determine borders of unexpected phase values region by analyzing wavelet transform of unwrapped phase map profiles. The borders of defect area are found by examining the convergence at fine scales of lines of wavelet modulus maxima. To have a physical interpretation of this convergence, second derivate of a Gaussian is employed as mother wavelet: estimated borders of defect region are some maximal curvature points of unwrapped phase map profile. To finish, we show that shearing amount does not affect estimated defect size with our methodology. So, shearography is adapted to quantify defects in shearing direction. Currently, in any other direction, an ambiguity exists on the position where the local estimation of defect width is performed. The methodoly cannot be employed.

Keywords: Shearography, defect size, wavelet transform, NDT

1. INTRODUCTION

Shearography is a recognized interferometric technique in industrial applications to measure the gradient of displacements, when displacements derivate is in the range of the ratio between the employed wavelength λ and the shearing amount.[1] To measure the gradient of displacements and not the displacements themself as many other interferometric techniques (holographic or speckle interferometries[2,3]), shearography consists in shearing the object beam in two partially overlapped beams, the overlap inducing the interference of the two beams. The two beams correspond to the arms of the interferometer: one can be interpreted as the reference beam for the other one, and inversely.

The irradiance I of the interference is given by the relation

$$I = 2I_0.[1 + \gamma.\cos(\phi)], \tag{1}$$

where I_0 is the average irradiance of the beams, γ is the visibility of the interference and ϕ is the phase difference between the two interfering beams.

By recording at least three phase shifted interferograms with a well-known phase shift α, the phase difference ϕ can be estimated.[4] Generally, the phase-shifting is realized by employing a piezo-transducer or a liquid crystal display. With $\alpha = \pi/2$ and a four-buckets algorithm, the recorded interferograms give the equations system

$$\begin{cases} I_1 = 2I_0\,[1 + \gamma.\cos(\phi)] \\ I_2 = 2I_0\,[1 + \gamma.\cos(\phi + \pi/2)] \\ I_3 = 2I_0\,[1 + \gamma.\cos(\phi + \pi)] \\ I_4 = 2I_0\,[1 + \gamma.\cos(\phi + 3\pi/2)] \end{cases} \tag{2}$$

E-mail: f.michel@deios.com, Telephone: +32 (0)4 372 93 09, Fax: +32 (0)4 372 93 17
DEIOS web page: www.deios.com, HOLOLAB web page: www.phg.ulg.ac.be/Hololab

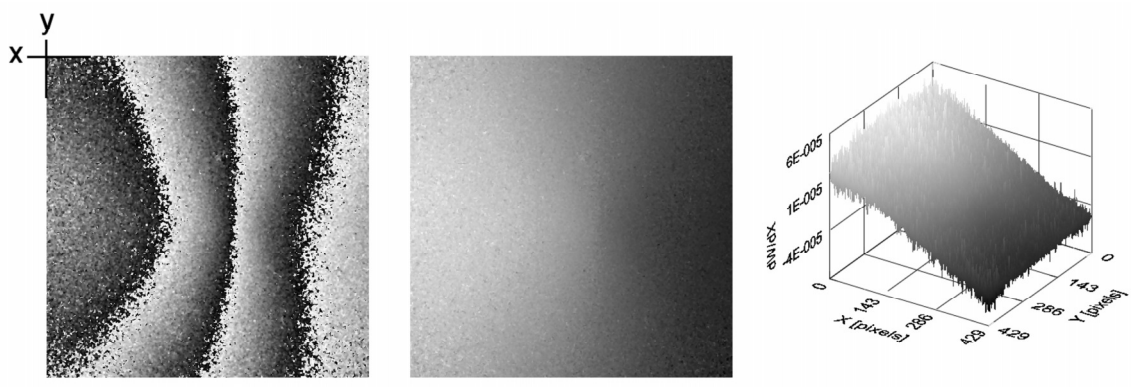

Figure 1. Left to right: wrapped phase map, unwrapped phase map and spatial out-of-plane displacement derivate distribution. A mean mask 3x3 has been applied to wrapped phase map at Sinus/Cosinus level before unwrapping. The phase unwrapping is based on a growing region algorithm.[6] The shearing is in the X direction and its amount is 8.4 mm. $\lambda = 532nm$.

with I_i, the irradiance of the ith recorded interferogram. The phase difference is then estimated with the relation[4]

$$\phi = \arctan \frac{I_4 - I_2}{I_1 - I_3}. \tag{3}$$

By estimating ϕ before and after a strain application, and by subtracting these phase estimations, we obtain a wrapped phase map Δ whose fringes are iso-phase curves, modulo 2π. A continuous spatial phase distribution Δ_d is then obtained by unwrapping this wrapped phase map.[5] In shearography, and if the shearing amount is small, the unwrapped phase map Δ_d is linked to the gradient of displacements by the relation[1]

$$\Delta_d = \left[\left(\overrightarrow{K_s}.\overrightarrow{e_x} \right) \frac{\partial u}{\partial x_i} + \left(\overrightarrow{K_s}.\overrightarrow{e_y} \right) \frac{\partial v}{\partial x_i} + \left(\overrightarrow{K_s}.\overrightarrow{e_z} \right) \frac{\partial w}{\partial x_i} \right] \delta x_i, \tag{4}$$

where $\overrightarrow{K_s}$ is the sensitivity vector of the setup; u, v, w are the components of the displacement vector; $\overrightarrow{e_x}$, $\overrightarrow{e_y}$, $\overrightarrow{e_z}$ are the unity vectors in the X, Y and Z directions; x_i is the shearing direction and δx_i is the shearing amount in the x_i direction.

If the sensibility vector is perpendicular to the object plane (X, Y), the x and y components of $\overrightarrow{K_s}$ are equal to zero. The Equation (4) is reduced to Equation (5) and only the gradient of out-of-plane displacements are analyzed:

$$\Delta_d = \left(\overrightarrow{K_s}.\overrightarrow{e_z} \right) \frac{\partial w}{\partial x_i} \delta x_i. \tag{5}$$

To clarify theoretical ideas described previously, an example of phase maps obtained by an out-of-plane displacements derivate measurement is resumed in Figure 1. The experience refers to charging a spherical 12 g mass on the center of a steel plate.[7] The employed setup is an almost-common path shearographic interferometer using the separation of the polarization states.[8]

Shearography allows to measure the gradient of displacements. So if the studied object has defects that affect surface displacements, then wrapped phase map presents singular fringes, and the unwrapped phase map has unexpected phase values regions. So shearography can be employed in non destructive testing (NDT). Figure 2 shows an example of NDT by shearography. The defect is a cavity of 10 x 10 x 5 mm^3 on the back side of a steel plate with a thickness of 7 mm. The applied strain is a 10 s during infrared radiation created by a 250 Watts IR lamp placed at 10 cm from the front of the plate. The deformed state of the object is an instant t_{relax} of the thermal relaxation after turning off the IR lamp. Many other NDT examples can be found in literature.[1,9,10]

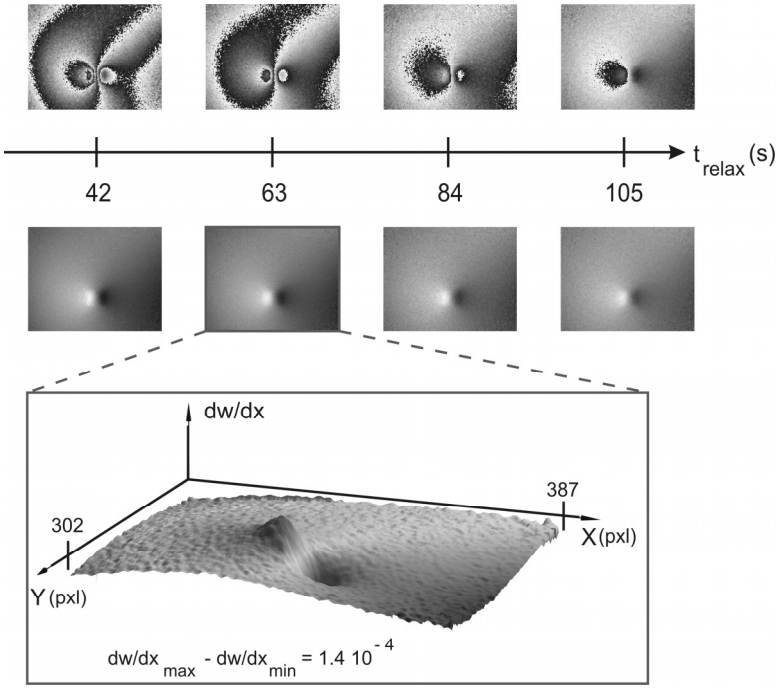

Figure 2. Wrapped and unwrapped phase maps, filtered by a 3x3 mean mask at Sinus/Cosinus level, of defected steel plate, at different t_{relax} instants. $\delta x = 6.2$ mm.

Literature and previous example attest that shearography is an interresting technique to detect defects. In this paper, we will show that shearography can also be employed to estimate the length of defects in the shearing direction. In Sect. 2, we present the general idea of the methodology, for a shearing in the X direction. In Sect. 3 and 4, we implement a wavelet transform based algorithm to carry out the methodology and we apply it to an experimental NDT example. In Sect. 5, we analyze the influence of the shearing amount on the estimated defect length. We conclude that shearography can be employed to quantify defect size in the shearing direction. In any other direction, currently, methodology cannot be employed because there is an ambiguity on the position where the local estimation of defect size is performed, if the defect shape is not previously known. Finally, note that the methodology described in this paper can be adjusted to be employed in many other interferometric techniques.

2. METHODOLOGY TO QUANTIFY DEFECTS DETECTED BY SHEAROGRAPHY

A detected defect is characterized in unwrapped phase map by an unexepected phase values region. On the profile $y = y_d$ of the unwrapped phase map, designed by $\Delta_d^{y=y_d}(x)$, the defect is included between the borders, x_1 and x_2, of the unexpected phase values area, see Figure 3. So, the defect length *in the sheared image*, i.e. the detector plane, and at $y = y_d$ level, $L(y_d)$, is estimated by the relation

$$L(y_d) = x_2(y_d) - x_1(y_d); x_2(y_d) > x_1(y_d). \tag{6}$$

In the non-sheared image, i.e. in the original object image, and for a shearing parallel to the X direction, the length of the defect is shorter than $L(y_d)$, because $L(y_d)$ is the length of the two basic sheared defects union. In the non-sheared image, the defect length in the shearing direction is estimated by the Equation 7, see Figure 4.

$$L^{obj}(y_d) = x_2^{obj}(y_d) - x_1^{obj}(y_d) = L(y_d) - \delta x. \tag{7}$$

$L^{obj}(y_d)$ is not the geometric, i.e. physical, defect length, but is the length of the impact region of the physical defect. In this paper, no difference is done between these two notions, because in practice the impact region of the physical defect is the critical region of the object.

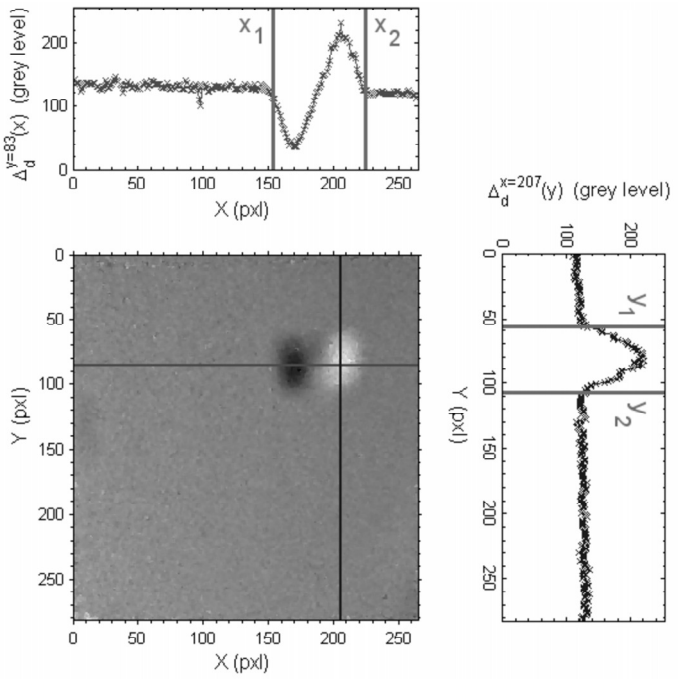

Figure 3. Unwrapped phase map of a wood plate with a 15 x 15 x 1 mm^3 cavity. The thickness of the plate is 8 mm. $\delta x = 55$ mm. The applied strain is a 2 s during radiation by a IR lamp (250 Watts) placed at 30 cm from the front of the wood plate. $t_{relax} = 15$ s.

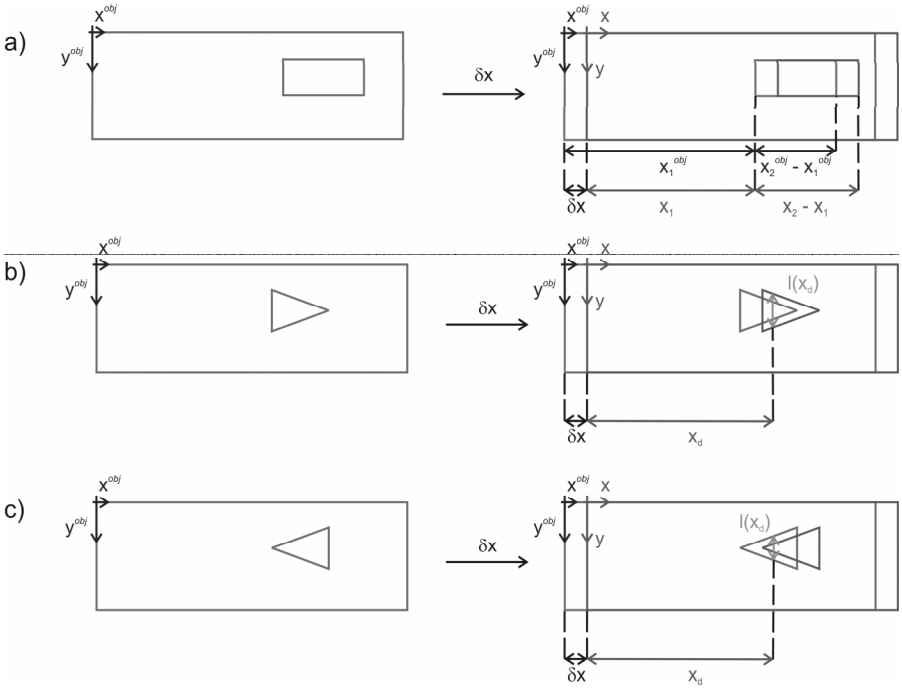

Figure 4. Left: non-sheared image of an object. The big rectangle is the object. The small one and the triangle are defects. Right: sheared image of the left image. a) matching between $L(y_d)$ and $L^{obj}(y_d)$. b) $x_d^{obj} = x_d$. c) $x_d^{obj} = x_d + \delta x$.

By analogy, defect is delimited at $x = x_d$ level by two borders, $y_1(x_d)$ and $y_2(x_d)$, and the defect width on this level, $l(x_d)$, is given *in the sheared image* by the Equation 8, see Figure 3.

$$l(x_d) = y_2(x_d) - y_1(x_d), y_2(x_d) > y_1(x_d). \tag{8}$$

In the non-sheared image and for a X shearing direction, the width $l^{obj}(x_d)$ is equal to the previous estimated width $l(x_d)$. No correction δx must be done because we are in the direction perpendicular to the shearing one. Unfortunatly, currently, an ambiguity exists on the estimated width. We cannot say where the estimation is done in the non-sheared image because in this last one, the estimation is done at $x_d^{obj} = x_d$ or at $x_d^{obj} = x_d + \delta x$, depending if defect is wider at $x_d^{obj} = x_d$ or at $x^{obj} = x_d + \delta x$, respectively, see Figure 4. The presented methodology cannot currently be employed to locally estimate the defect size in the direction perpendicular to the shearing one.

In practice, it is necessary to have a completely objective and repeatable estimations of x_1 and x_2 borders. By considering that these borders correspond to some important phase variations of the signal $\Delta_d^{y=y_d}(x)$, they can be estimated with a wavelet transform based algorithm, because wavelet transform is acknowledged to be highly capable to detect important variations and/or singularities of a signal.[11–14] The employed wavelet transform algorithm is presented in Sect. 3.

Note that the presented methodology can also be employed in many other interferometric techniques as speckle interferometry. In this case, there is not sheared image and we have $L^{obj}(y_d) = L(y_d)$, $l^{obj}(x_d) = l(x_d)$ and the ambiguity relative to x_x does not exist: $x_d^{obj} = x_d$.

3. INTEGRATION OF THE METHODOLOGY WITH A WAVELET TRANSFORM MODULUS MAXIMA BASED ALGORITHM

A wavelet $\Psi(x)$ is a function that should satisfy the admissibility criteria[11]

$$\int_{-\infty}^{+\infty} \Psi(x)dx = 0. \tag{9}$$

This wavelet, the mother wavelet, is dilated with given s scaling factors and translated with given u position terms to give a lot of functions $\Psi_{u,s}(x)$, named daughter wavelets,[11]

$$\Psi_{u,s}(x) = \frac{1}{\sqrt{s}}\Psi\left(\frac{x-u}{s}\right). \tag{10}$$

The daughter wavelets are the basis functions of the transform, i.e. the wavelet transform of a f(x) signal consists in making the convolution between the daughter wavelets and the signal. The wavelet coefficient Wf(u,s) at the x = u position and at the s scale is given by the relation[11]

$$Wf(u,s) = \int_{-\infty}^{+\infty} f(x)\Psi_{u,s}^*(x)dx, \tag{11}$$

where * symbol designs the conjugate complex.

To determine the important variations of a signal f(x), the methodology consists in[11–14]:

1. calculating the wavelet coefficients for all desired (u, s) couples;
2. determining the local maxima of the modulus of the wavelet transform per s scale. The local maxima of the modulus of the wavelet transform are the coefficients Wf(u,s) verifying $|Wf(u_0, s_0)| > |Wf(u_0 \pm 1, s_0)|$;
3. building the trajectories of local maxima in the (u, s) plane by connecting the closest maxima which belong to two consecutive values of s;

4. analyzing the convergence of these trajectories to fine s scales. The convergence points u are the position of the singularities or/and of the important variations of the studied signal.

In this kind of application, the employed wavelets are real, e.g. the derivates of a Gaussian. The complex wavelets, e.g. Morlet Wavelets, are usually used to analyze the frequencies evolution of the signal.[15–18] The derivates of a Gaussian can be interpreted as multiscale differential operators[11] : if the mother wavelet is the n^{th} derivate of a Gaussian, then Wf(u, s) is the n^{th} derivate of signal at x = u, calculated on a s spatial domain width. If the mother wavelet is the first derivate of a Gaussian, the wavelet coefficients are the slopes of the signal. If the mother wavelet is the second derivate of a Gaussian, the wavelet is named mexican hat and the wavelet coefficients are the curvatures of the signal. We will employ the mexican hat as mother wavelet. The estimated borders x_1 and x_2 shall be interpreted as some maximum curvature points of f(x). The normalized mexican hat mother wavelet $\Psi(x)$ is defined by the relation[11]

$$\Psi(x) = \frac{2\sqrt[4]{\pi}}{\sqrt{3}}(x^2-1)exp\left(\frac{-x^2}{2}\right) \tag{12}$$

and the daughter walelets are

$$\Psi_{u,s}(x) = \frac{2\sqrt[4]{\pi}}{\sqrt{3}}\frac{1}{\sqrt{s}}\left(\left(\frac{x-u}{s}\right)^2-1\right)exp\left(-\frac{(x-u)^2}{2s^2}\right). \tag{13}$$

In summarise, to find the borders x_1 and x_2 of the defect on the profile $y = y_d$ of the unwrapped phase map, $\Delta_d^{y=y_d}(x)$, we calculate the wavelet transform of the signal $\Delta_d^{y=y_d}(x)$ with the mexican hat wavelet, we determine the local modulus maxima of this transform, we analyze the trajectories of these local modulus maxima in the (u, s) plane and we estimate the convergence of these trajectories at fine s scales.

4. APPLICATION OF THE METHODOLOGY

Apply the previously described methodology on the $\Delta_d^{y=83}(x)$ signal of the unwrapped phase map presented in Figure 3. The first step in our methodology consists in calculating the wavelet transform of the signal, with the mexican hat mother wavelet. The normalized wavelet coefficient modulus $\left|W\Delta_d^{y=83}(x)\right|$ are showed in Figure 5. In this (u, s) plane, the unexpected phase values are represented by four ridges. The first one is relative to the curvature in the x_1 neighborood, the second one is connected to the curvature of the signal minimum, the third one is linked to the curvature of signal maximum and the last one is concerning the curvature in the neightborood of x_2, according to the interpretation of the mexican hat mother wavelet.

The wavelet transform being calculated, the second step in the methodology consists in determining the local coefficient modulus maxima of every s values. The wavelet coefficient $W\Delta_d^{y=83}(u,s)$ is a modulus maximum if $\left|W\Delta_d^{y=83}(u,s)\right| > \left|W\Delta_d^{y=83}(u\pm1,s)\right|$. Every local modulus maximum belonging to $s = s_0$ line of the (u, s) plane is then connected to the nearest modulus maximum of the $s = s_0 - 1$. This construction of the trajectories of the modulus maxima is guaranteed and relatively simple, because the wavelets are derivated from a Gaussian. For this kind of wavelet, the modulus maxima lines are always continuous along the s scales (Hummel, Poggio and Yuille proposition[11]). In Figure 5, the right image represents the trajectories of the maxima of the wavelet transform modulus seen in left image.

Theoretically, the x_1 and x_2 borders are respectively the u values where the modulus maxima lines of the first and fourth ridges, $T_{x_1}(u,s)$ and $T_{x_2}(u,s)$, converge to fine scales, e.g. s = 1 pxl. Unfortunatly, with experimental data, the fine scales are confused, because they are relative to the noise of the signal. Consequently, the convergence of the trajectories are defined as the u values of the modulus maxima lines at a cut-off spatial frequency, $1/s_c$. To work with a cut-off frequency adapted to the signal noise ratio, s_c is determined by the number of new trajectories that appear along the s scales, see Figure 6. By convention, we define s_c as the wavelet size for which one the number of new trajectories is just smaller or equal to 5% of the total number of modulus maxima lines: $s_c = 6$ pxl, in the presented example.

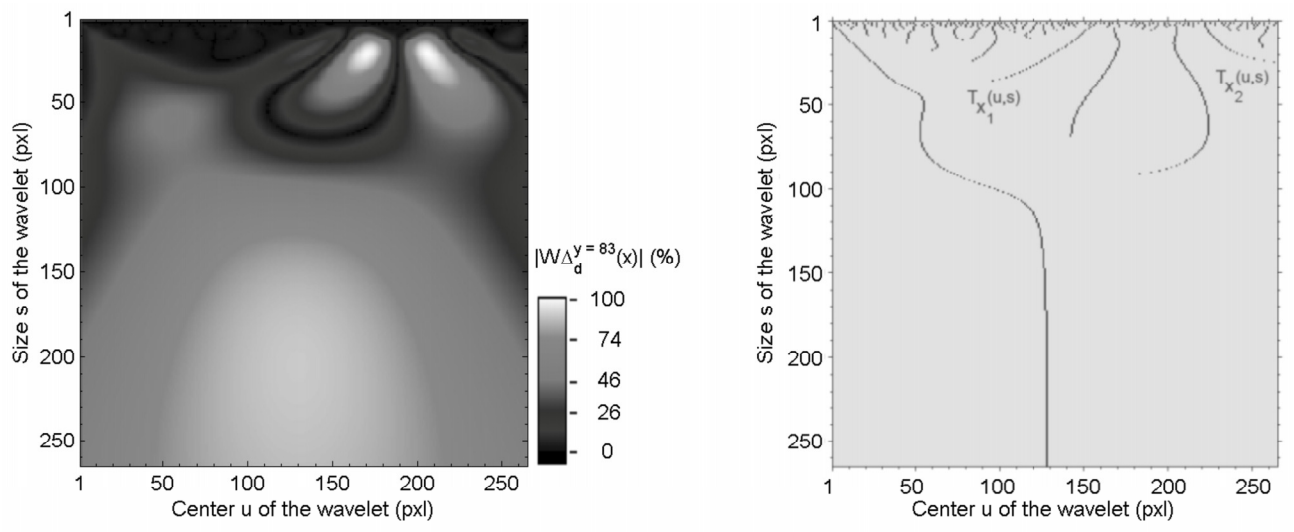

Figure 5. Left: normalized wavelet coefficient modulus of $\Delta_d^{y=83}(x)$ signal. Right: modulus maxima lines of the wavelet transform. The $T_{x_1}(u,s)$ and $T_{x_2}(u,s)$ trajectories are employed to estimate the position of the borders x_1 and x_2, respectively.

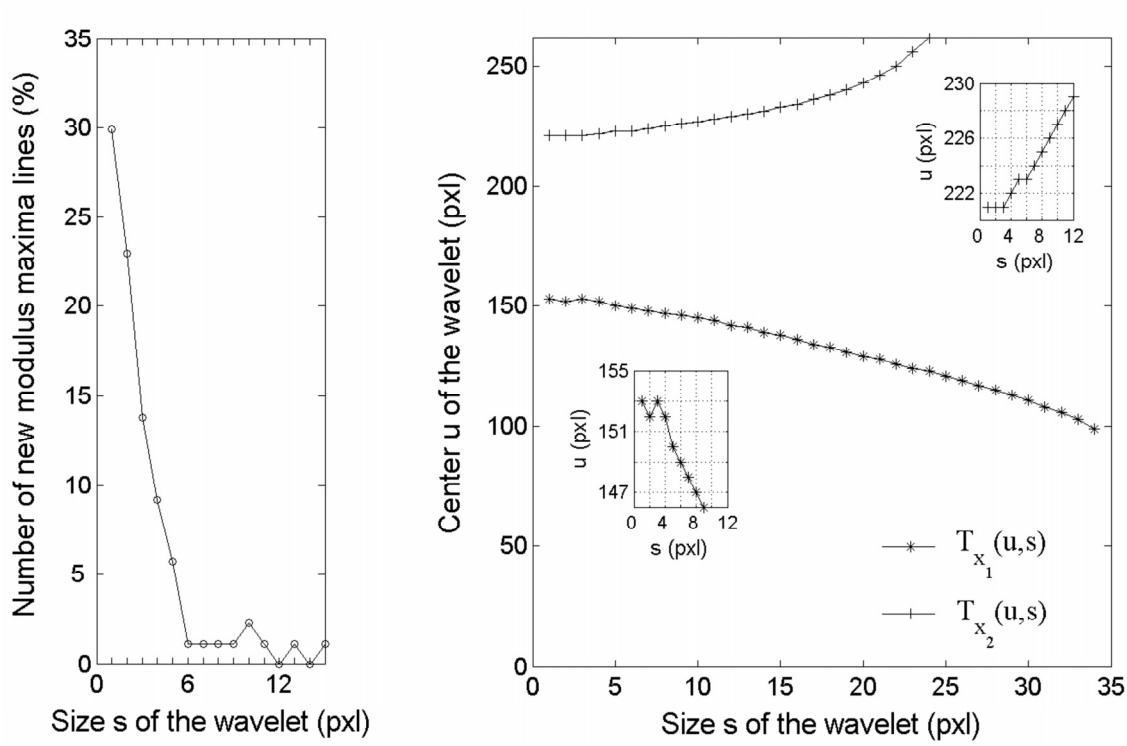

Figure 6. Left: number of new modulus maxima trajectories in function of the wavelet size and given in purcent of total number of modulus maxima lines. Right: trajectories $T_{x_1}(u,s)$ and $T_{x_2}(u,s)$ employed to estimate the x_1 and x_2 borders of the unexpected phase values region.

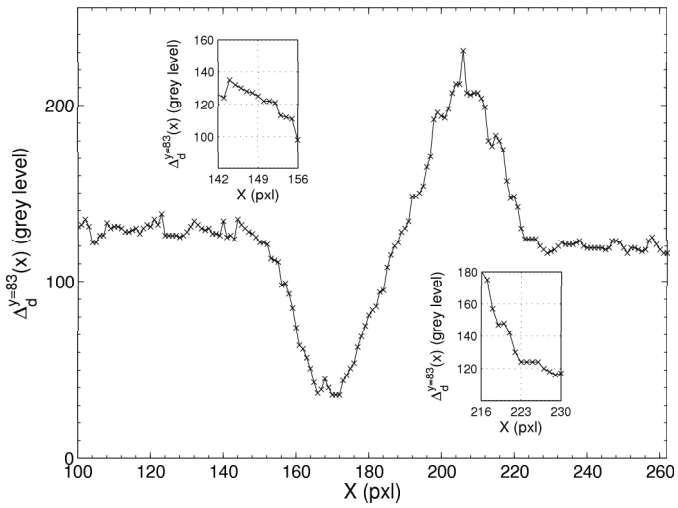

Figure 7. Putting in emphasis of the estimated unexpected phase values region borders of the studied $\Delta_d^{y=83}(x)$ signal: $x_1 = 149$ pxl and $x_2 = 225$ pxl.

With a 1/6 pxl^{-1} cut-off frequency, the convergence of the trajectories $T_{x_1}(u,s)$ and $T_{x_2}(u,s)$ is respectively equal to 149 pxl and 223 pxl, see Figure 6. The borders of the unexpected phase values area are then 149 pxl and 223 pxl, see Figure 7. That induces $L(y = 83) = 74$ pxl.

The calibration of the interferometer states that one pixel is equal to 0.29 mm and the shearing amount is 5.51 mm. So the size of the defect impact region, $L^{obj}(y = 83)$, is 15.95 mm. The theoretical physical, e.g. geometric, defect length is 15.0 mm.

5. INFLUENCE OF THE SHEARING AMOUNT

The defect studied in the Sect. 4 has been detected with some different shearing amounts. For each of them, some phase maps have been calculated for different IR radiation times, t_{IR}, and t_{relax} instants. Considering several (t_{IR}, t_{relax}) couples allows to have a statistical sample of phase maps for the defect size estimation and for every shearing amount.

The shearing amount affects the sensibility of the setup. The average distance L_{ext} between the extrema of the unexpected phase values region of the $\Delta_d^{y=83}(x)$ signal is function of the shearing amount,[10] see Figure 8.

However, the shearing amount does not affect the average estimated defect length, see Figure 8. The shearing amount has been introduced as corrective term in Equation 7. So, finally shearography can be employed to estimate defect size in the shearing direction, if the employed methodology takes account of the shearing amount, as it is the case in the methodology presented in this paper.

6. CONCLUSION

In conclusion, a methodology has been presented to quantify, in the shearing direction, the size of defects detected by shearography. A wavelet transform modulus maxima based algorithm has been implemented to carry out the methodology. The technique has then been applied to experimental examples in which well known defects have been studied. It allows to estimate the defect with an relative error smaller than 10 %. In a last step, the influence of the shearing amount on the estimated defect length has been studied. It appears that the shearing amount affects the sensibility of the interferometer, but does not affect the estimation of the defect size, because the shearing amount has been introduced in our equations. Note that the methodology can be employed in many other interferometric technique as speckle interferometry.

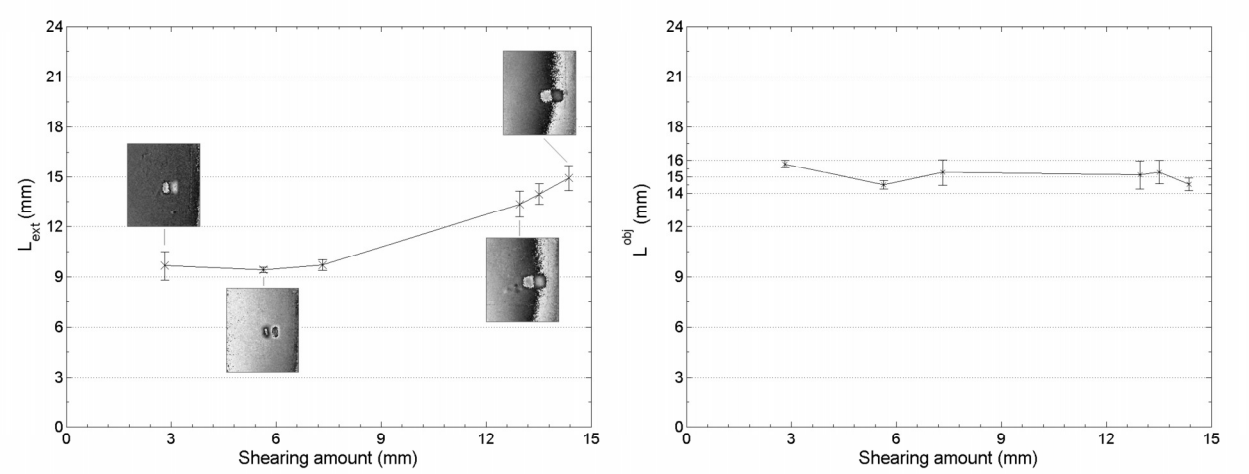

Figure 8. Left: average distance between the signal extrema in function of the shearing amount. Right: influence of the shearing amount on the average estimated defect length in the shearing direction. The error bars represent standard deviations of the statistic analyze.

ACKNOWLEDGMENTS

Fabrice MICHEL is supported by a "FIRST Entreprise" Project and Dr. Vincent MOREAU, by a "RIT" Project granted by the Research Depart. of the "Région Wallonne" (Belgium). The authors also thank Drs. RENOTTE and LION from HOLOLAB laboratory for their daily advices.

REFERENCES

1. W. Steinchen and L. Yang, *Digital Shearography* (SPIE Press, Bellingham, 2003).
2. R. Jones and C. Wykes, *Holographic and Speckle Interferometry* (Cambridge U. Press, 1989).
3. P. K. Rastogi, *Digital Speckle Pattern Interferometry and Related Techniques* (John Wiley & Sons, Chichester, 2001).
4. K. CREATH, "Phase-shifting speckle interferometry", Applied Optics **24**(18), 3053-3058 (1985).
5. D. C. Ghiglia and M. D. Pritt, *Two-Dimensional Phase Unwrapping: Theory, Algorithms, and Software* (John Wiley & Sons, New-York, 1998).
6. A. Baldi, "Phase unwrapping by region growing", Applied Optics **42**(14), 2498-2505 (2003).
7. V. Rosso, L. Zhang, F. Michel, Y. Renotte, Y. Lion, A-M Habraken, "Out-of-plane displacement derivate measurement: comparison of results obtained by a shearographic interferometer using the separation of the polarization states and the finite element method", in *Photonics North 2006*, P. Mathieu Ed. (Proc. SPIE 6343, 2006) 634327.
8. V. Rosso, F. Michel, V. Moreau, Y. Renotte, B. Tilkens, Y. Lion, An almost-common path shearographic interferometer using the separation of the polarization states, in Speckle06: Speckles, From Grains to Flowers, P. Slangen and C. Cerruti Eds. (Proc. SPIE 6341, 2006) 634111.
9. L. Yang, F. Chen, W. Steinchen, M. Y. Hung, "Digital Shearography for Nondestructive Testing: Potentials, Limitations and Applications", Journal of Holography and Speckle **1**(2), pp. 69-79 (2004).
10. K-S. Kim, K-S Kang, Y-J Kang, S-K Cheong, "Analysis of an internal crack of pressure pipeline using ESPI ans shearography", Optics and Laser Technology 35 (2003) 639-643.
11. S. Mallat, *A Wavelet Tour of Signal Processing* (Academic Press, 1999).
12. J. A. Newburry, C. T. Russell, "Shock profile analysis using wavelet transform", J. Geophys. Rev. 103, 6503-6511, 1998.
13. T. Figarella, M. H. Jansen, "Brush wear detection by continuous wavelet transform", Mechanical Systems and Signal Processing **21**(3), pp 1212-1222, 2007.

14. Z. K. Peng, F. L. Chu, P. W. Tse, "Singularity analysis of the vibration signals by means of wavelet modulus maxima method", Mechanical Systems and Signal Processing **21**(2), pp 780-794, 2007.
15. C. J. Tay, Y. Fu, "Determination of curvature and twist by digital shearography and wavelet transforms", Optics Letters **30**(21), 2005.
16. L. R. Watkins, S. M. Tan, T. H. Barnes, "Determination of interferometer phase distributions by use of wavelets", Optics Letters **24**(13), 1999.
17. J. Zhong, J. Weng, "Spatial carrier-fringe pattern analysis by means of wavelet transform: wavelet transform profilometry", Applied Optics **43**(26), 2004.
18. R-S Chang, J-Y Sheu C-H Lin, H-C Liu, "Analysis of CCD moiré pattern for micro-range measurements using the wavelet transform", Optics and Laser Technology 35 (2003) 43-47.